Minireview

Visible-light optical coherence tomography-based multimodal system for quantitative fundus autofluorescence imaging

Zahra Nafar[1], Rong Wen[2] and Shuliang Jiao[1]

[1]Department of Biomedical Engineering, Florida International University, Miami, FL 33174, USA; [2]Bascom Palmer Eye Institute, University of Miami Miller School of Medicine, Miami, FL 33136, USA
Corresponding author: Shuliang Jiao. Email: shjiao@fiu.edu

Impact statement

Quantitative fundus autofluorescence imaging with simultaneous visible-light optical coherence tomography-based multimodal technology has potential significant impact on the diagnosis and monitoring the progression of retinal diseases.

Abstract

Fundus autofluorescence (FAF) imaging is commonly used in ophthalmic clinics for diagnosis and monitoring of retinal diseases. Lipofuscin in the retinal pigment epithelium (RPE), with A2E as its most abundant component and a visual cycle by-product, is the major fluorophore of FAF. Lipofuscin accumulates with age and is implicated in degenerative retinal diseases. The amount of lipofuscin in RPE can be assessed by quantitative measurement of FAF. However, the currently available FAF imaging technologies are not capable of quantifying the absolute intensity of FAF, which is essential for comparing images from different individuals, and from the same individual over time. One major technical difficulty is to compensate the signal attenuation by ocular media anterior to the RPE (pre-RPE media). FAF intensity is also influenced by fluctuations in imaging conditions such as illumination power and detector sensitivity, all of which need to be compensated. In this review, we present the concept and research progress of using visible-light optical coherence tomography-based simultaneous multimodal retinal imaging to compensate signal attenuation by pre-RPE media and the influence of parameters of the acquisition system for accurate measurement of FAF intensities.

Keywords: Visible-light optical coherence tomography, retinal pigment epithelium lipofuscin, fluorescence quantification, fundus autofluorescence imaging, retinal imaging, multimodal imaging

***Experimental Biology and Medicine* 2018; 243: 1263–1272. DOI: 10.1177/1535370218813529**

Introduction

The retinal pigment epithelium (RPE) is a monolayer of pigmented cells located between photoreceptors and the choroid.[1–3] It maintains the normal function of photoreceptors, including regenerating 11-cis retinal in the visual cycle[4] and phagocytosis of the shed photoreceptor outer segment tips.[5] The RPE also helps to enhance vision by absorbing scattered light with melanin. As part of the blood-retina barrier, the RPE selectively facilitates material exchange between the retina and the bloodstream in the choroid.[6,7] Furthermore, RPE cells secrete a variety of growth factors to maintain the integrity of the underlying choroid and overlying photoreceptors.[8] Given the functional importance of the RPE to photoreceptors and the retina, dysfunction of the RPE would inevitably affect the retina, the photoreceptors, and the vision.

Lipofuscin is a complex lipid/protein aggregate of non-degradable end products from phagocytosis of shed photoreceptor outer segments in the RPE.[9] It is the major source of fundus autofluorescence (FAF) and accumulates with age,[10,11] thus it can serve as a biomarker of RPE aging. Lipofuscin affects RPE cells in many ways, including generation of oxidants and free radicals leading to oxidative damage,[12–16] lysis of cell membrane,[17,18] light-induced apoptosis,[19,20] and photo-oxidation-associated complement activation.[21,22] These effects are believed to contribute to the pathogenesis of age-related macular degeneration (AMD), as well as other retinal dystrophies.[11,23,24]

FAF was first detected in a vitreous fluorophotometry study.[25] It is a measure of fluorophores mainly contained in the lipofuscin granules in the RPE.[26,27] Evidence has shown that A2E, a by-product of the photoreceptor visual cycle,[28–30] is the major fluorophore in lipofuscin granules and the major fluorophore of FAF.[11] FAF imaging has been used for the diagnosis and monitoring the progression of AMD, Stargardt disease, RPE tear, choroideremia, and

retinal drug toxicity,[31,32] while the major focus of FAF clinical studies is on non-neovascular AMD.[33,34] AMD is a major cause of irreversible blindness in the elderly population. Globally, the projected number of AMD patients is 196 million in 2020 and 288 million in 2040.[35] In the US, the number of AMD patients is projected to increase from 2.1 million in 2010 to 3.7 million in 2030.[36]

The currently available FAF imaging techniques, which are based on confocal scanning laser ophthalmoscopy[22,37–39] and fundus photography,[40,41] are not capable of quantifying the absolute FAF intensities[22] although different imaging techniques have their corresponding advantages and disadvantages. Without knowing the absolute intensities of a FAF image, it is difficult to compare FAF images from different individuals, and even images from the same individual taken over time. Delori *et al*.[20] developed an innovative method by using a fluorescence reference to calculate the intensity of measured FAF. A fluorescence reference target of known fluorescence efficiency was placed in the intermediate retinal imaging plane covering a small portion of the field of view (FOV) and was imaged whenever a FAF image is taken. However, this method can quantify measured FAF intensities, but not the true quantities. The excitation and emitted fluorescence light are attenuated when it travels through the pre-RPE media, including the cornea, the aqueous humor, the lens, and the vitreous. The attenuation coefficient differs among different individuals. The pre-RPE media also changes over time in an individual, especially the lens.[42]

The multimodal visible-light optical coherence tomography (VIS-OCT) and FAF (VIS-OCT–FAF) imaging technology, which simultaneously acquires OCT and FAF images with a single broadband light source, offers a unique opportunity to achieve true quantification of absolute FAF intensities. The simultaneously acquired VIS-OCT image of the RPE carries the same attenuation information as that incurred to the FAF image. The depth-resolving capability of OCT allows segmentation of signals from the RPE, which can be used as an internal reference so that the attenuation effect of tissues anterior to the RPE can be removed and true intensities of FAF can be quantified using a reference fluorescent target as described by Delori and co-workers.

Simultaneous VIS-OCT and FAF imaging

The first VIS-OCT-based simultaneous multimodal imaging system was described in 2012,[43] which used a single broadband light source with a center wavelength of 415 nm and a bandwidth of 8 nm. The light source was provided by frequency doubling of an ultra-fast Ti:Sapphire laser (Micra-5, center wavelength: 800 nm, maximum bandwidth: 120 nm) by using a barium borate crystal. For the first time, the technology demonstrated the concept of providing intrinsically registered OCT and fluorescence microscopy for simultaneous structural and molecular imaging. A supercontinuum (SC) laser was used as the light source in a newer version of VIS-OCT–FAF, in which a center wavelength of 488 nm was selected to be compatible with the FAF imaging systems currently in use.[44] The VIS-OCT axial resolution was significantly improved from 12 to 5.6 μm in air by using a 20 nm bandwidth.

In all these imaging systems, the OCT signals were detected in the spectral domain with a spectrometer. The fluorescence signals were detected with a PMT in a confocal arrangement. A near-infrared OCT (NIR-OCT) was also integrated in the systems for alignment purpose before image acquisition to avoid visible light exposure to the eye during the alignment process. Since the OCT and FAF images were generated by the same group of photons the speed of the two imaging modalities is the same, which is limited by the speed of the CCD/CMOS camera used for OCT or the PMT for the fluorescence.

The system was tested on rats for simultaneous *in vivo* OCT and FAF imaging. The technology successfully imaged the same group of rats over time to reveal the accumulation of lipofuscin with age. Histograms of the AF intensities in Figure 1 show a shift of distribution toward higher intensities with age. The technology has also been demonstrated of imaging exogenous fluorophores by imaging fluorescein angiography of rat eyes as shown in Figure 2.

Eliminating attenuation factors in FAF imaging

It was recently demonstrated that simultaneously acquired VIS-OCT images can be used to compensate illuminating power fluctuations and attenuation factors for FAF images with VIS-OCT–FAF system,[45] a step further toward the quantification of the absolute FAF intensities.

To test the concept, a phantom was built to simulate light attenuation by media to RPE (Figure 3(a)). It had a plastic weighing dish to hold fluorescein solution to simulate lipofuscin. The fluorescein solution was covered by a

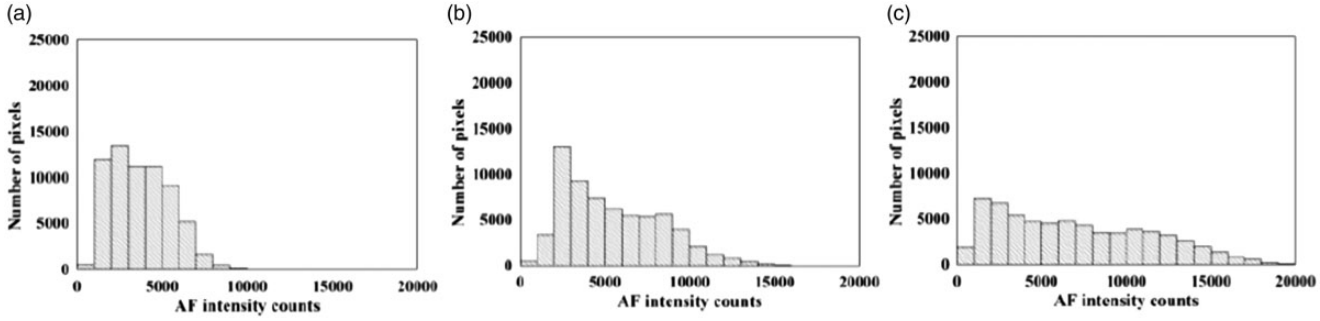

Figure 1. Histograms of *in vivo* FAF imaging of rats over time for four weeks.[39] (a) 10 week old, (b) 12 week old, and (c) 14 week old. AF: autofluorescence.

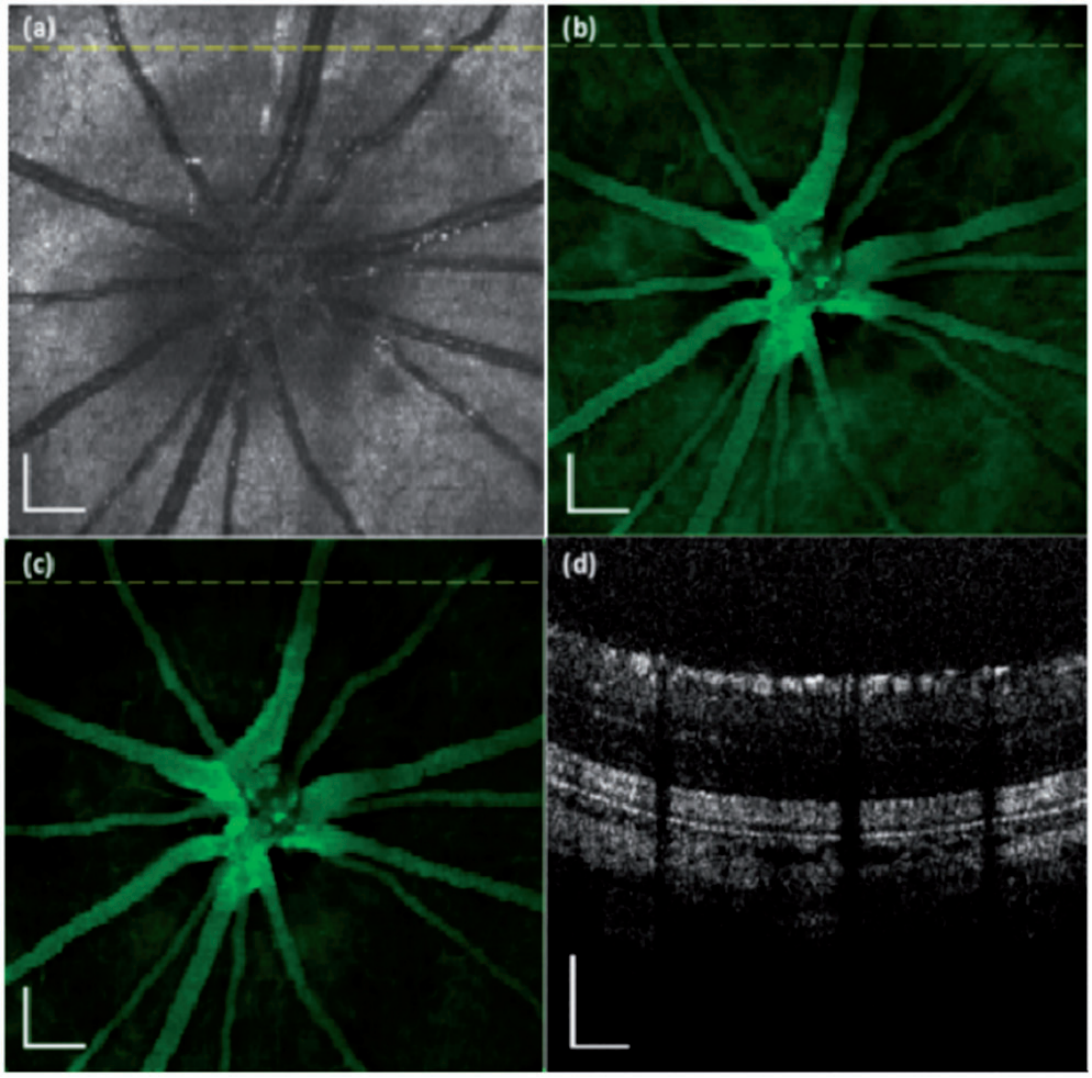

Figure 2. VIS-OCT and FA images simultaneously acquired from a rat retina *in vivo*. (a) OCT fundus image, (b) FAF image, (c) AF/OCT compensated fundus image, and (d) OCT B-scan. The dotted line in the OCT fundus image marks the location of the OCT B-scan image. Bar: 200 μm.[45] (A color version of this figure is available in the online journal.)

transparent polystyrene membrane to control the thickness of the sample. A set of ND filters (nominal OD values of 0.1–0.5) was placed in front of the phantom to introduce light attenuation. As the attenuation (OD value) increased, significant decreases were detected in the fluorescence intensity (Figure 3(b), blue line) and OCT signal intensity from the second boundary (Figure 3(b), red line). But the normalized AF signals (Figure 3(b), green line) showed only a gradual linear decrease, which was proved to be caused by bleaching of the dye, as the measurement sequence was from low to high OD values.

To further test the effect of normalizing the FAF image intensity with that of the simultaneously acquired OCT image, the system was applied in imaging rat retina. FAF and VIS-OCT images were obtained from four albino rats (10 weeks old) every two weeks for four weeks. The average FAF intensity counts were normalized with the RPE OCT signal intensities by manually segmenting the RPE layer and averaged over the entire imaged area. The normalized AF intensity was calculated as $I_{AF}/I_{OCT\text{-}RPE}$, where I_{AF} is the raw averaged FAF intensity and $I_{OCT\text{-}RPE}$ is the averaged intensity of the RPE OCT signals. Unlike the raw intensities (Figure 3(c)), the normalized data show that the rates of increase among animals are very similar (Figure 3 (d)), indicating that lipofuscin in those animals increased at a similar rate and linearly correlated with age which is consistent with previous findings.[46–48] Note that the 'levels' of I_{AF} in Figure 3(d) between animals are not normalized to a common reference, and thus they cannot be compared quantitatively. Since the detectors for OCT and the FAF are independent, the ratio $I_{AF}/I_{OCT\text{-}RPE}$ cannot cancel the factors of detector sensitivity. As a result, further development by using standard reference targets for OCT and FAF is necessary.

VIS-OCT–FAF system with standard reference targets

To quantify true FAF intensities, the effects of the excitation light intensity and detector sensitivity need to be

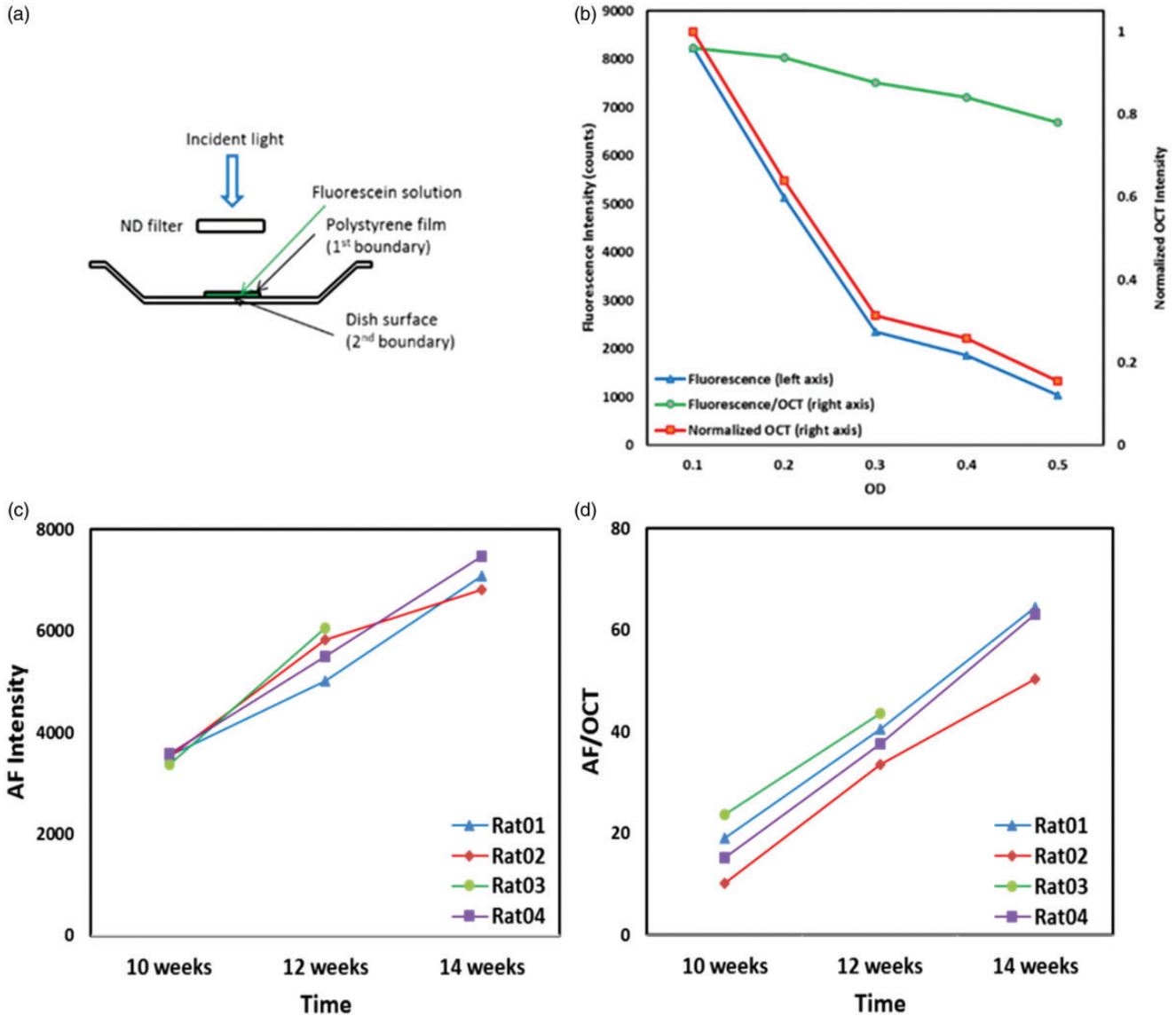

Figure 3. (a) Phantom experiment design; (b) simultaneous OCT, AF, and AF/OCT with different OD values; (c) average of FAF of rats over time; and (d) average of FAF/OCT of rats over time.[45] AF: autofluorescence; ND: Neutral Density; OCT: optical coherence tomography. (A color version of this figure is available in the online journal.)

eliminated, which can be addressed by using a fluorescence standard with known fluorescence efficiency and a reflection standard with known reflectance in the intermediate retinal imaging plane. When imaged together these two reference standards can build a quantitative relationship between the FAF and VIS-OCT image intensities. The absolute intensities of AF from the RPE can be calculated using the OCT and the AF signals from the RPE and the standard references, assuming the attenuation of the AF signals is approximately the same as that of the OCT signals from the ocular media. With true intensities quantified by the multimodal imaging technology, it is possible to compare FAF images from different eyes and from the same eye at different time points.[45,49,50]

Figure 4 shows a schematic of the imaging system, which consists of an optical fiber-based NIR- (red line) and VIS-OCT (blue line).[50] The NIR-OCT uses a superluminescent diode centered at 840 nm and the VIS-OCT uses a SC laser (filtered output: 480 ± 15 nm) as the light source. The probe light of the two OCT systems in the sample arm is combined by a dichroic mirror, scanned and delivered to the eye by the same optical system. Two reference standard targets were implemented in the intermediate retinal imaging plane, covering around 14% of the bottom of the FOV (Figure 5(a)). The fluorescence reference is the same as the one introduced by Delori *et al.*[2] (Microscopy Education, Texas Red) and the reflectance reference (Microscopy Education, DAPI) consists of the same substrate material with fluorescence peak off the detection range. To achieve VIS-OCT imaging of the reference target along with the retina, the reference arm of the VIS-OCT system is split into two arms by a non-polarizing beam splitter. The shorter path length is to capture the interference signal from the reference target and the longer path corresponds to imaging the retina. A computer-controlled shutter blocks the light while the retina is scanned and is opened when the

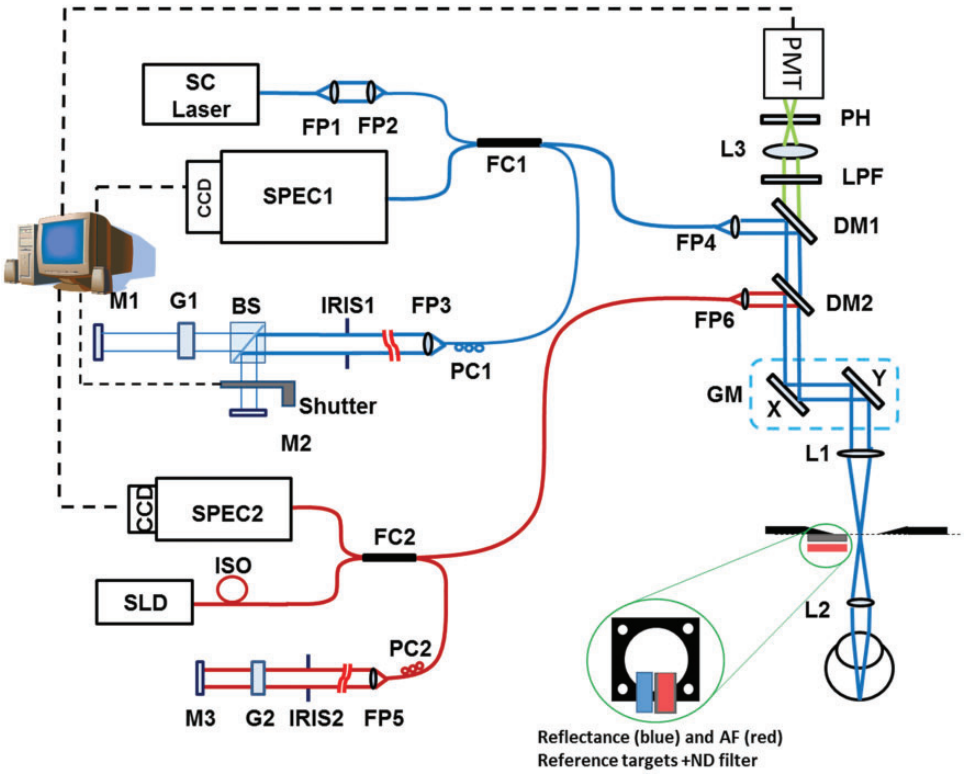

Figure 4. Schematic of the simultaneous VIS-OCT and AF imaging system: VIS-OCT (blue), NIR-OCT (red) and AF (green). BS: beam splitter; DM1-2: dichroic mirrors; FC1-2: fiber coupler; FP1-6: collimation fiber ports; G1-2: BK7 glass plates; GM: galvanometer scanner; IRIS1-2: iris; ISO: isolator; L1-3: lens; LPF: long-pass filter; M1-3: reference arm mirrors; ND filter (OD: 10); PC1-2: polarization controller; PH: pinhole; PMT: photo multiplier tube; SC: supercontinuum; SLD: superluminescent diode; SPEC1-2: spectrometer.[50] (A color version of this figure is available in the online journal.)

raster scan reaches the reference target position. The fluorescence reference target is cemented to a ND filter with a total optical density of 10 (roundtrip OD: 20), to reduce the fluorescence intensity to the level of rodent retina. The FAF was detected by a PMT module in a confocal arrangement with a 25 μm diameter pinhole and a long pass filter (FGL515M, cut-on wavelength: 515 nm, Thorlabs). The NIR- and VIS-OCT signals were detected in the spectral domain by their corresponding spectrometers.

The simultaneous VIS-OCT and FAF with two standard reference targets were tested on rat retina *in vivo*. Figure 5 shows the images of a 14-month-old albino rat together with the two reference targets at the bottom. The *en face* projection of the RPE reflectance signal (Figure 5(c)) was provided by manual segmentation of the RPE layer.

Quantitative FAF imaging and system calibration

Theoretical model. The reflectance model proposed by Van de kraats *et al.*[51] indicates that the reflected light from the eye can be categorized into three regions of reflectance: pre-RPE media, RPE layer, and post-RPE media. With the depth-resolving capability of VIS-OCT, we can extract the reflectance of the RPE layer from the OCT images through segmentation. The AC component of the OCT interference signal is proportional to the square root of the sample reflectance, and we have

$$R_{OCT} = I_{AC}^2 / I_{DC} \propto R_s I_s \tag{1}$$

$$R_{OCT-RPE} = I_0 \tau_{pre}^2(\lambda)\left[1-\rho_{pre}(\lambda)\right]^2 \rho_{RPE}(\lambda)\frac{\pi}{4}\alpha^2 \tag{2}$$

$$R_{OCT-R} = I_0 \rho_R(\lambda)\frac{\pi}{4}\alpha' \tag{3}$$

where R_{OCT}, $R_{OCT\text{-}RPE}$, and $R_{OCT\text{-}R}$ are the expressions for the OCT signal, the reflectance from the RPE, and the reflectance from the reference target; I_{DC} and I_{AC} refer to the AC and DC components of OCT interference signal; τ and ρ are transmittance and reflectance, respectively; α and α' are the solid angles comprising the light, respectively, from retina and reference target. Subscripts RPE and 'pre' refer to retinal pigmented epithelium and pre-RPE media, respectively. The AF intensity from the RPE and the reference target can be expressed as

$$I_{FAF} = I_0 \tau_{pre}^2(\lambda)\left[1-\rho_{pre}(\lambda)\right]^2 \xi_{RPE} A_d \frac{\pi}{4}\alpha^2 \tag{4}$$

$$I_{RAF} = I_0 \xi_R A_d \frac{\pi}{4}\alpha'^2 \tag{5}$$

where ξ_{RPE} and ξ_R are fluorescence efficiencies of RPE lipofuscin and reference target, respectively. A_d represents detector sensitivity.

It is obvious that by normalizing the VIS-OCT reflectance and FAF of the RPE layer to those of the reference targets, factors related to the light intensity and detector sensitivity

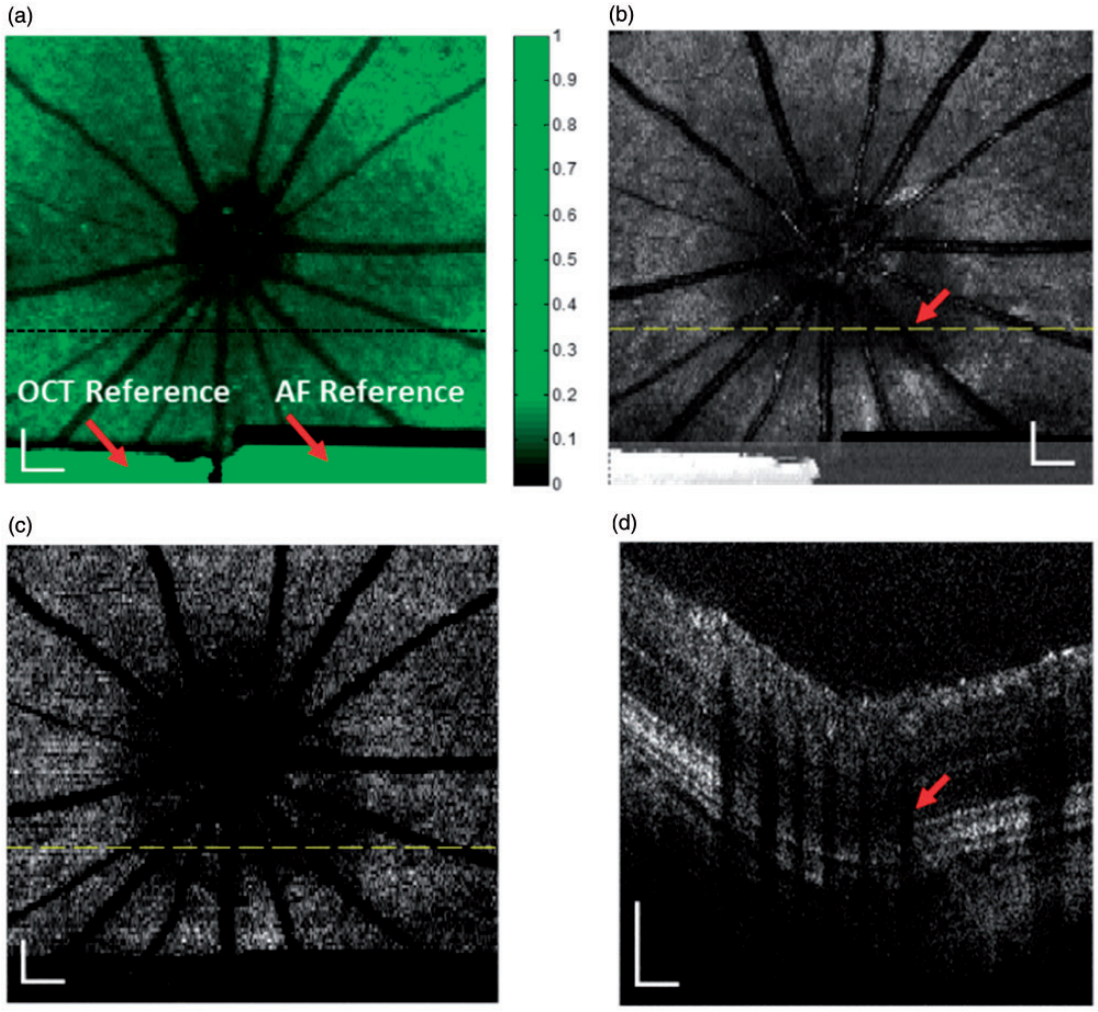

Figure 5. Simultaneous fundus AF and OCT images of a 14-month-old albino rat. (a) AF image normalized to the fluorescence reference, (b) fundus OCT projection normalized to the reflectance reference, (c) *qOCT* projection of the segmented RPE, and (d) OCT B-scan at the location marked with a yellow dashed line. Bar: 200 μm.[50]

will be eliminated. However, the attenuation terms in both signals are remained. Finally, assuming similar transmittance of the ocular media in excitation and emission wavelengths,[52] by dividing the normalized FAF (*qAF*) with normalized VIS-OCT reflectance of the RPE layer (*qOCT*), these factors will be also eliminated. We have

$$\frac{I_{FAF}/I_{RAF}}{R_{OCT-RPE}/R_{OCT-R}} = \frac{qAF}{qOCT} = \frac{C_L Q_L \varepsilon_L d_{RPE}/C_R Q_R \varepsilon_R d_R}{\rho_{RPE}/\rho_R} \quad (6)$$

where C, Q, ε, and d, are concentration, quantum yield, extinction coefficient, and effective thickness of the fluorescent layer, respectively.

Phantom experiment. We conducted phantom experiments to validate the theoretical model. A model eye consisting of a lens, a master fluorescence slide as the retina, and a set of ND filters simulating the pre-RPE attenuation was built. Two different master fluorescence slides with different fluorescence materials (FITC and Texas Red) were tested. The model eye was imaged at different illumination power and detector sensitivity and the detected signals are shown in Figures 6 and 7. The calibration results in Figures 6(b) and (c) and 7(b) showed that in the calculated *qOCT* and *qAF*, the illumination power effects on both VIS-OCT and FAF signals, and the effects of detector sensitivity on detected FAF signals can be eliminated. Furthermore, as shown in Figure 7(c) and (d) *qAF*/*qOCT* is independent of the OD values of the ND filters, indicating that the ratio can effectively compensate the attenuation by pre-RPE media.

In vivo imaging. We tested the VIS-OCT–FAF system by imaging rat retinas *in vivo*. *qAF*/*qOCT* was calculated in three groups of animals: two-month albino (n = 5), 14-month albino (n = 6), and 12-month pigmented rats (n = 6). The reflectance projection of the RPE layer was obtained by manual segmentation on the OCT B-scans. The average RPE reflectance was calculated in a square window within a controlled distance from the optic disc and without blood vessel shadows. The *qAF* was obtained by normalizing the averaged AF signal of the retina to the

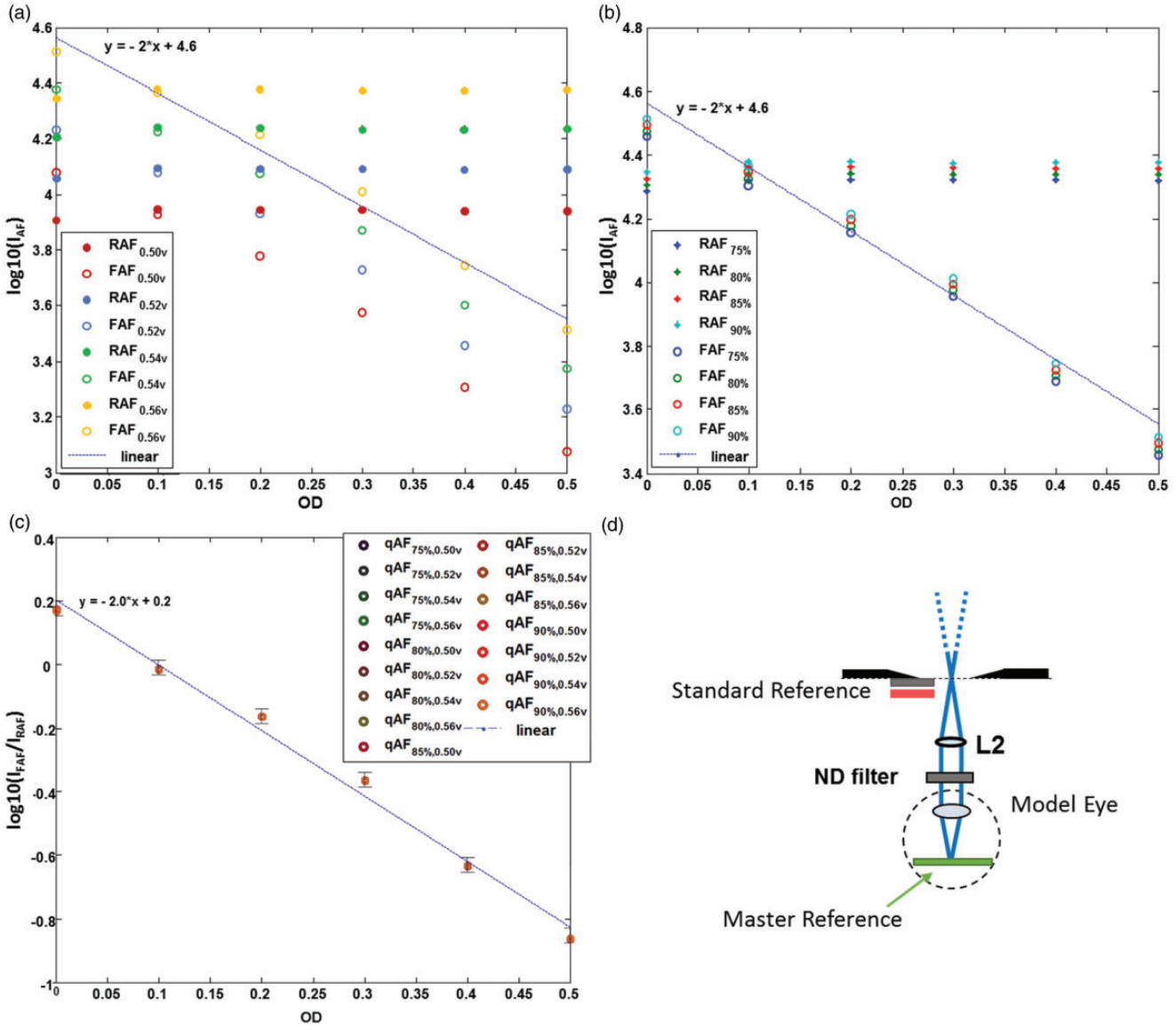

Figure 6. Quantitative AF signals from the model eye (master reference: FITC) and the standard reference at different imaging conditions. (a) AF signals versus OD value of the ND filter in front of the model eye at 90% light source power and different PMT control voltage (0.50–0.56 V), (b) AF signals versus OD value of the ND filter in front of the model eye at fixed PMT control voltage (0.56 V) and different light source power (75–90% output power), (c) the calculated log10(FAF/RAF) versus OD value of the ND filter in front of the model eye at all the different imaging conditions, and (d) schematic of the model eye used in the experiments.[50] FAF: Fundus autofluorescence; ND: Neutral Density; OD: Optical Density; qAF: quantified autofluorescence; RAF: Reference autofluorescence.

AF signal of the reference target, and *qOCT* was calculated by normalizing averaged OCT reflectance signal of the RPE layer to the reflectance standard target.

As shown in Figure 8, 14-month-old albino rats have significantly higher *qAF* ($p = 0.0063$) and *qAF*/*qOCT* ($p = 0.0325$) levels than two-month-old albinos, indicating accumulation of lipofuscin.[45] The *qAF* is significantly lower in 12-month pigmented rats than 14-month albino rats ($p = 0.0019$), consistent with previous studies.[53] The OCT reflectance of the segmented RPE layer in pigmented rats is also significantly lower than the 14-month albino rats. Consequently, no significant difference is found in the *qAF*/*qOCT* ratios between the two groups of rats ($p = 0.8021$).

These results indicate that the VIS-OCT–FAF system is capable of detecting true FAF intensity. The finding that the true FAF level is comparable to the albino rats of similar age when *qAF* is normalized with *qOCT*, even though the raw *qAF* in pigmented rats is much lower than the albino rats, suggests that the system can compensate signal attenuation by RPE melanin as well. Thus, *qAF*/*qOCT* is also independent of the amount of melanin in the RPE. This feature of the VIS-OCT–FAF system could have great clinical significance.

Future prospective

The theoretical analysis and experimental results clearly demonstrate that the simultaneous VIS-OCT–FAF technology is capable of measuring the absolute and true intensities of FAF. However, the technology needs to be further refined and optimized. For example, there is a

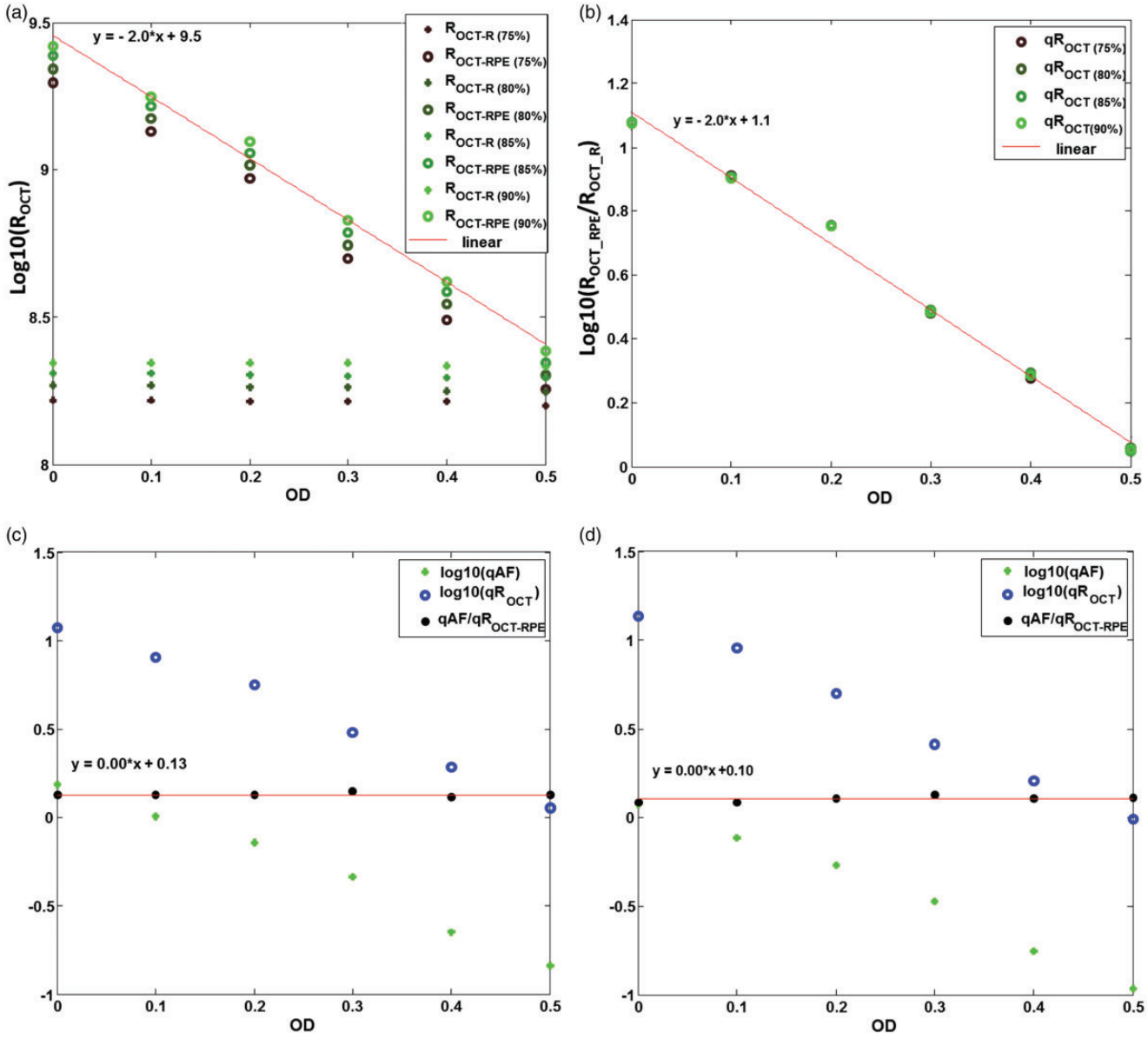

Figure 7. OCT reflectance signals from the model eye (master reference: FITC) at different OD values of the ND filter and from the standard reference at different imaging conditions. (a) The source power was changed from 75 to 90%; (b) OCT reflectance of the model eye normalized to the reference target (*qOCT*) for the data in (a); (c) *qAF*, *qOCT*, and *qAF*/*qOCT* ratio; and (d) *qAF*, *qOCT*, and *qAF*/*qOCT* ratio for the model eye with the Texas Red slide at the retinal plane.[50] OCT: optical coherence tomography; qAF: quantified autofluorescence; RPE: retinal pigment epithelium.

compensation/scaling factor in the calculated *qAF*/*qOCT* in relation to the concentration of the fluorophore in the simulated retinal RPE, or RPE lipofuscin in the eye *in vivo*, as indicated in the results shown in Figure 7(c) and (d). This compensation/scaling factor may be related to the optics of the imaging system and the geometric parameters of the eye, such as the pupil size. This compensation/scaling factor can be determined in phantom studies with controlled parameters.

Visible light illumination is more likely to cause eye movement and introduce motion artifacts in the FAF images. An effective measure to reduce motion artifacts is to increase the imaging speed. Currently, our latest multimodal imaging system is capable of acquiring both images in less than 1 s while the alignment process is guided by using a NIR-OCT. The short time visible light exposure with light intensity in the safety level will not alter lipofuscin deposition in the RPE cells.

The standard reference target used in the VIS-OCT–FAF system discussed above was from a commercial source with a fluorescence efficiency too high for FAF detection that a high optical density (OD = 10) ND filter had to be employed. The high OD value made it impossible to image the fluorescence target with OCT. Furthermore, the emission and excitation spectrums of the commercial reference target with Texas Red are not the same as those of RPE lipofuscin/A2E, and the quantum yield of Texas Red is much higher than A2E. An ideal standard reference target should have a fluorescence efficiency in the range of FAF so that a single reference target can be used for both OCT and

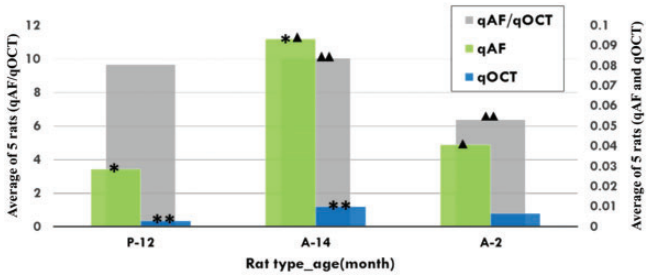

Figure 8. Comparison of the *qAF*, *qOCT*, and *qAF/qOCT* in three groups of albino and pigmented rats.[50] qAF: quantified autofluorescence; qOCT: quantified OCT (optical coherence tomography).

FAF, and with a fluorophore having similar emission and excitation spectrum, as well as quantum yield to those of A2E.

We have been working on a reference target using synthesized A2E as the fluorophore embedded in a polymethyl methacrylic slide to serve as a common reference target for both imaging modalities. Standard reference target with synthesized A2E as the fluorophore will simplify the calculation of absolute FAF intensities. In addition, we propose to introduce a new intensity unit as a measure of FAF intensity. This new unit, A2E equivalent unit, or AEU, is defined as one AEU equivalent to the fluorescent intensity of 1 ng/mm^2 of A2E emitted from RPE. The use of AEU to measure the intensity of FAF will not only provide a standard for FAF measurement, but also give us a sense of how much A2E-like fluorophores, and thus the amount of lipofuscin, are present in the retina. A reference target using synthesized A2E as the fluorophore will make it easier to adopt AEU as FAF intensity unit.

FAF, a biological phenomenon, carries information that likely reflects the health status of the RPE and the retina. Detection of FAF has been used widely in ophthalmology clinics. The VIS-OCT–FAF technology is being developed with the capability of quantitative measurement of the absolute intensities of FAF overcomes the limitations of the technologies currently available. With absolute FAF intensities embedded in FAF images, it is possible to compare FAF images from different individuals or from the same individual over time can be compared. This new technology will be a clinical tool to provide information that was previously inaccessible to ophthalmologists for better patient care.

Authors' contributions: SJ initiated and supervised the project. ZN performed the experiments and analyzed the results. SJ, RW, and ZN discussed the results and contributed to the manuscript.

DECLARATION OF CONFLICTING INTERESTS

The author(s) declared no potential conflicts of interest with respect to the research, authorship, and/or publication of this article.

FUNDING

Institutes of Health (NIH) (R01EY026643, R01EY018586, and P30-EY014801).

ORCID iD

Zahra Nafar http://orcid.org/0000-0002-6680-4234

REFERENCES

1. Zhou J, Kim SR, Westlund BS, Sparrow JR. Complement activation by bisretinoid constituents of RPE lipofuscin. *Invest Ophthalmol Vis Sci* 2009;**50**:1392–9
2. Delori F, Greenberg JP, Woods RL, Fischer J, Duncker T, Sparrow J, Smith RT. Quantitative measurements of autofluorescence with the scanning laser ophthalmoscope. *Invest Ophthalmol Vis Sci* 2011;**52**:9379–90
3. Johnson EJ. Age-related macular degeneration and antioxidant vitamins: recent findings. *Curr Opin Clin Nutr Metab Care* 2010;**13**:28–33 Jan
4. Nowak JZ. Age-related macular degeneration (AMD): pathogenesis and therapy. *Pharmacol Rep* 2006;**58**:353
5. Yung M, Klufas MA, Sarraf D. Clinical applications of fundus autofluorescence in retinal disease. *Int J Retina Vitreous* 2016;**2**:12
6. Holz F, Bird AC, Schmitz-Valckenberg S, Spaide R. *Atlas of fundus autouorescence imaging*. Berlin: Springer-Verlag; 2007
7. Bindewald A, Bird AC, Dandekar SS, Dolar-Szczasny J, Dreyhaupt J, Fitzke FW, Einbock W, Holz FG, Jorzik JJ, Keilhauer C, Lois N, Mlynski J, Pauleikhoff D, Staurenghi G, Wolf S. Classification of fundus autofluorescence patterns in early age-related macular disease. *Invest Ophthalmol Vis Sci* 2005;**46**:3309–14
8. Bindewald A, Schmitz-Valckenberg S, Jorzik JJ, Dolar-Szczasny J, Sieber H, Keilhauer C, Weinberger AW, Dithmar S, Pauleikhoff D, Mansmann U, Wolf S, Holz FG. Classification of abnormal fundus autofluorescence patterns in the junctional zone of geographic atrophy in patients with age related macular degeneration. *Br J Ophthalmol* 2005;**89**:874–8
9. Wong WL, Su X, Li X, Cheung CMG, Klein R, Cheng CY, Wong TY. Global prevalence of age-related macular degeneration and disease burden projection for 2020 and 2040: a systematic review and meta-analysis. *Lancet Glob Health* 2014;**2**:e106–16
10. National Eye Institute. *Age-related macular degeneration (AMD)*, https://nei.nih.gov/eyedata/amd/tables (accessed 24 September 2018)
11. Sparrow JR, Nakanishi K, Parish CA. The lipofuscin fluorophore A2E mediates blue light–induced damage to retinal pigmented epithelial cells. *Invest Ophthalmol Vis Sci* 2000;**41**:1981–9
12. Solbach U, Keilhauer C, Knabben H, Wolf S. Imaging of retinal autofluorescence in patients with age-related macular degeneration. *Retina* 1997;**17**:385–9
13. Holz FG, Bellman C, Staudt S, SchüTt F, VöLcker HE. Fundus autofluorescence and development of geographic atrophy in age-related macular degeneration. *Invest Ophthalmol Vis Sci* 2001;**42**:1051–6
14. Morgan JI, Hunter JJ, Masella B, Wolfe R, Gray DC, Merigan WH, Delori FC, Williams DR. Light-induced retinal changes observed with high-resolution autofluorescence imaging of the retinal pigment epithelium. *Invest Ophthalmol Vis Sci* 2008;**49**:3715–29
15. Delori FC, Fleckner MR, Goger DG, Weiter JJ, Dorey CK. Autofluorescence distribution associated with drusen in age-related macular degeneration. *Invest Ophthalmol Vis Sci* 2000;**41**:496–504
16. Spaide RF. Fundus autofluorescence and age-related macular degeneration. *Ophthalmology* 2003;**110**:392–9
17. Gray DC, Merigan W, Wolfing JI, Gee BP, Porter J, Dubra A, Twietmeyer TH, Ahamd K, Tumbar R, Reinholz F, Williams DR. In vivo fluorescence imaging of primate retinal ganglion cells and retinal pigment epithelial cells. *Opt Express* 2006;**14**:7144–58
18. Roorda A, Duncan JL. Adaptive optics ophthalmoscopy. *Annu Rev Vis Sci* 2015;**1**:19–50
19. Morgan JI, Dubra A, Wolfe R, Merigan WH, Williams DR. In vivo autofluorescence imaging of the human and macaque retinal pigment epithelial cell mosaic. *Invest Ophthalmol Vis Sci* 2009;**50**:1350–9
20. Delori F, Keilhauer C, Sparrow JR, Staurenghi G, Holz F, Schmitz-Valckenberg S. Origin of fundus autofluorescence. In: Holz F., Spaide R., Bird A., Schmitz-Valckenberg S. (eds) *Atlas of fundus autouorescence imaging*. Berlin Heidelberg: Springer-Verlag, 2007, pp.17–29

21. Pokorny J, Smith VC, Lutze M. Aging of the human lens. *Appl Opt* 1987;**26**:1437–40
22. Boulton M, Wassell J. *Ageing of the human retinal pigment epithelium*. In: Coscas G., Piccolino F.C. (eds) *Retinal pigment epithelium and macular diseases*. Dordrecht: Springer-Dordrecht, 1998, pp.19–28
23. Foster PJ, Buhrmann R, Quigley HA, Johnson GJ. The definition and classification of glaucoma in prevalence surveys. *Br J Ophthalmol* 2002;**86**:238–42
24. Tham Y, Li X, Wong TY, Quigley HA, Aung T, Cheng C. Global prevalence of glaucoma and projections of glaucoma burden through 2040: a systematic review and meta-analysis. *Ophthalmology* 2014;**121**:2081–90
25. Sparrow JR, Zhou J, Ben-Shabat S, Vollmer H, Itagaki Y, Nakanishi K. Involvement of oxidative mechanisms in blue-light-induced damage to A2E-laden RPE. *Invest Ophthalmol Vis Sci* 2002;**43**:1222–7
26. Ben-Shabat S, Parish CA, Vollmer HR, Itagaki Y, Fishkin N, Nakanishi K, Sparrow JR. Biosynthetic studies of A2E, a major fluorophore of retinal pigment epithelial lipofuscin. *J Biol Chem* 2002;**277**:7183–90
27. Winkler BS, Boulton ME, Gottsch JD, Sternberg P. Oxidative damage and age-related macular degeneration. *Mol Vis* 1999;**5**:32
28. De S, Sakmar TP. Interaction of A2E with model membranes. Implications to the pathogenesis of age-related macular degeneration. *J Gen Physiol* 2002;**120**:147–57
29. Sparrow JR, Cai B, Jang YP, Zhou J, Nakanishi K. A2E, a fluorophore of RPE lipofuscin, can destabilize membrane. In: Hollyfield J.G., Anderson R.E., LaVail M.M. (eds) *Retinal degenerative diseases*. Boston: Springer-Boston, 2006, pp.63–68
30. SchüTt F, Davies S, Kopitz J, Holz FG, Boulton ME. Photodamage to human RPE cells by A2-E, a retinoid component of lipofuscin. *Invest Ophthalmol Vis Sci* 2000;**41**:2303–8
31. National Eye Institute. *Glaucoma*, https://nei.nih.gov/eyedata/glaucoma/tables (accessed 24 September 2018)
32. Friedman DS, Wolfs RC, O'Colmain BJ, Klein BE, Taylor HR, West S, Leske MC, Mitchell P, Congdon N, Kempen J. Eye diseases prevalence research group. Prevalence of open-angle glaucoma among adults in the United States. *Arch Ophthalmol* 2004;**122**:532–8
33. Kamal DS, Viswanathan AC, Garway-Heath DF, Hitchings RA, Poinoosawmy D, Bunce C. Detection of optic disc change with the Heidelberg retina tomograph before confirmed visual field change in ocular hypertensives converting to early glaucoma. *Br J Ophthalmol* 1999;**83**:290–4
34. Chauhan BC, Blanchard JW, Hamilton DC, LeBlanc RP. Technique for detecting serial topographic changes in the optic disc and peripapillary retina using scanning laser tomography. *Invest Ophthalmol Vis Sci* 2000;**41**:775–82
35. Weinreb RN, Dreher AW, Coleman A, Quigley H, Shaw B, Reiter K. Histopathologic validation of Fourier-ellipsometry measurements of retinal nerve fiber layer thickness. *Arch Ophthalmol* 1990;**108**:557–60
36. Bagga H, Greenfield DS, Feuer W, Knighton RW. Scanning laser polarimetry with variable corneal compensation and optical coherence tomography in normal and glaucomatous eyes. *Am J Ophthalmol* 2003;**135**:521–9
37. Bagga H, Greenfield DS. Retinal nerve fiber layer assessment using scanning laser polarimetry. *Int Ophthalmol Clin* 2004;**44**:29–42
38. Medeiros FA, Bowd C, Zangwill LM, Patel C, Weinreb RN. Detection of glaucoma using scanning laser polarimetry with enhanced corneal compensation. *Invest Ophthalmol Vis Sci* 2007;**48**:3146–53
39. Sehi M, Ume S, Greenfield DS. Scanning laser polarimetry with enhanced corneal compensation and optical coherence tomography in normal and glaucomatous eyes. *Invest Ophthalmol Vis Sci* 2007;**48**:2099–104
40. Wollstein G, Schuman JS, Price LL, Aydin A, Stark PC, Hertzmark E, Lai E, Ishikawa H, Mattox C, Fujimoto JG, Paunescu LA. Optical coherence tomography longitudinal evaluation of retinal nerve fiber layer thickness in glaucoma. *Arch Ophthalmol* 2005;**123**:464–70
41. Trick GL, Calotti FY, Skarf B. Advances in imaging of the optic disc and retinal nerve fiber layer. *J Neuroophthalmol* 2006;**26**:284–95
42. Huang X, Knighton RW, Cavuoto LN. Microtubule contribution to the reflectance of the retinal nerve fiber layer. *Invest Ophthalmol Vis Sci* 2006;**47**:5363–7
43. Dai C, Liu X, Jiao S. Simultaneous optical coherence tomography and autofluorescence microscopy with a single light source. *J Biomed Opt* 2012;**17**:0805021–3
44. Jiang M, Liu T, Liu X, Jiao S. Simultaneous optical coherence tomography and lipofuscin autofluorescence imaging of the retina with a single broadband light source at 480nm. *Biomed Opt Express* 2014;**5**:4242–8
45. Nafar Z, Jiang M, Wen R, Jiao S. Visible-light optical coherence tomography-based multimodal retinal imaging for improvement of fluorescent intensity quantification. *Biomed Opt Express* 2016;**7**:3220–9
46. Mann D, Yates P, Stamp J. The relationship between lipofuscin pigment and ageing in the human nervous system. *J Neurol Sci* 1978;**37**:83–93
47. West CD. A quantitative study of lipofuscin accumulation with age in normals and individuals with Down's syndrome, phenylketonuria, progeria and transneuronal atrophy. *J Comp Neurol* 1979;**186**:109–16
48. Delori FC, Goger DG, Dorey CK. Age-related accumulation and spatial distribution of lipofuscin in RPE of normal subjects. *Invest Ophthalmol Vis Sci* 2001;**42**:1855–66
49. Keane PA, Sadda SR. Retinal imaging in the twenty-first century: state of the art and future directions. *Ophthalmology* 2014;**121**:2489–500
50. Nafar Z, Wen R, Jiao S. Visible light OCT-based quantitative imaging of lipofuscin in the retinal pigment epithelium with standard reference targets. *Biomed Opt Express* 2018;**9**:3768–82
51. van de Kraats J, Berendschot TT, van Norren D. The pathways of light measured in fundus reflectometry. *Vision Res* 1996;**36**:2229–47
52. Boettner EA, Wolter JR. Transmission of the ocular media. *Invest Ophthalmol Vis Sci* 1962;**1**:776–83
53. Zhang X, Zhang HF, Puliafito CA, Jiao S. Simultaneous in vivo imaging of melanin and lipofuscin in the retina with photoacoustic ophthalmoscopy and autofluorescence imaging. *J Biomed Opt* 2011Aug; 16 (8): 080504